Large Exchange Bias after Zero-Field Cooling from an Unmagnetized State

B. M. Wang, Y. Liu, P. Ren, B. Xia, K. B. Ruan, J. B. Yi, J. Ding, X. G. Li, and L. Wang

Large exchange bias after zero-field cooling from an unmagnetized state

B. M. Wang,[1] Y. Liu,[1, *] P. Ren,[2] B. Xia,[2] K. B.

Ruan,[2] J. B. Yi,[3] J. Ding,[3] X. G. Li,[4] and L. Wang[2, †]

[1]*School of Mechanical and Aerospace Engineering,*

Nanyang Technological University, 639798, Singapore

[2]*Division of Physics and Applied Physics,*

School of Physical and Mathematical Sciences,

Nanyang Technological University, 637371, Singapore

[3]*Department of Materials Science and Engineering,*

National University of Singapore, 119260, Singapore

[4]*Hefei National Laboratory for Physical Sciences at Microscale and Department of Physics,*

University of Science and Technology of China, Hefei 230026, China

Abstract

Exchange bias (EB) is usually observed in systems with interface between different magnetic phases after *field cooling*. Here we report an unusual phenomenon in which a *large* EB can be observed in Ni-Mn-In bulk alloys after *zero-field cooling from an unmagnetized state*. We propose that this is related to the newly formed interface between different magnetic phases during the initial magnetization process. The magnetic unidirectional anisotropy, which is the origin of EB effect, can be created *isothermally* below the blocking temperature.

PACS numbers: 75.30.Et, 75.30.Gw, 75.50.Cc, 75.50. Lk

When a system consisting of ferromagnetic (FM)-antiferromagnetic (AFM) [1], FM-spin glass (SG) [2], AFM-ferrimagnetic (FI) [3], and FM-FI [4] interface is cooled with field through the Néel temperature (T_{N}) of the AFM or glass temperature (T_{SG}) of the SG, exchange bias (EB) is induced showing a shift of hysteresis loop [$M(\mathrm{H})$] along the magnetic field axis. Since its discovery by Meiklejohn and Bean in 1956 [1], EB has been extensively studied during the past fifty years, partly because of its applications in ultrahigh-density magnetic recording, giant magnetoresistance and spin valve devices [5, 6]. The EB effect is attributed to an FM unidirectional anisotropy formed at the interface between different magnetic phases [5]. Generally, the process of field cooling (FC) from higher temperature is used to obtain FM unidirectional anisotropy in different EB systems [1–4]. The FM unidirectional anisotropy can also be realized by depositing the AFM layer onto a saturated FM layer [5], by ion irradiation in an external magnetic field [7], by zero-field cooling (ZFC) with remnant magnetization [8, 9]. In a word, the FM unidirectional anisotropy in these EB systems is formed by *reconfiguring* the FM spins at the interface between different magnetic phases. Here, we named the previous EB generally observed after FC as the conventional EB (CEB). Furthermore, Saha *et al.* [10] argued that a small spontaneous EB observed after ZFC without remnant magnetization, which has been ignored or attributed to the experimental artifact, can be explained theoretically in an otherwise isotropic EB system. The CEB effect after FC has also been observed in NiMn-based Heusler bulk alloys, such as NiMnSn [11], NiMnSb [12], and NiMnIn [13], coexisting of AFM and FM phases. In this Letter, we report a large EB effect (the maximum EB field is about 1300 Oe at 10 K) after *ZFC from an unmagnetized state* in Ni-Mn-In bulk alloys. Namely, a large FM unidirectional anisotropy can be produced *isothermally*, which has never been reported to date and cannot be expected in the CEB systems [14].

The details of sample preparations and measurements for $\mathrm{Ni_{50}Mn_{50-x}In_x}$(NiMnIn$x$, $x =$ 11, 12, 13, 14 and 15) alloys are illustrated in the supplementary information [14]. Two measurement processes can be used to obtain a closed $M(\mathrm{H})$ loop after ZFC (only consider ($|+H| = |-H|$):

(1) P type, $0 \rightarrow (+H) \rightarrow 0 \rightarrow (-H) \rightarrow 0 \rightarrow (+H)$,

(2) N type, $0 \rightarrow (-H) \rightarrow 0 \rightarrow (+H) \rightarrow 0 \rightarrow (-H)$.

The first $0 \rightarrow (+H)/(-H)$ curve is called as an initial magnetization curve. Generally, these two kinds of measurement will obtain the same loop except for the initial magnetization

curve. Thus, only one of them has been used to obtain $M(H)$ loop in the previous studies. However, they will give the different results in the present study.

Figure 1(a) shows the temperature dependence of magnetization $[M(T)]$ of NiMnIn13 ($T_N \sim 410$ K) measured under $H = 10$ Oe after ZFC and FC. The ZFC curve exhibits a peak at $T_p = 53$ K and an irreversibility between ZFC and FC curves occurring at $T_f \sim$ 150 K, which is similar to that of NiCoMnSn [15]. The magnetic state of NiMnIn13 at low temperatures is superparamagnetic (SPM) domains embedded in AFM matrix as in NiCoMnSn. The SPM domains are collectively frozen forming a superspin glass (SSG) state at lower temperatures [15]. The $M(H)$ curve at 300 K is a straight line without any SPM/FM feature, which indicates that the T_c is at lower temperature [inset of Fig. 1(a)]. To further confirm this SSG state, we measured ac susceptibility at various frequencies (fs) with an ac magnetic field of 2.5 Oe after ZFC from 300 K. Figure 1(b) shows the temperature dependence of the real part of ac susceptibility. The T_p increases with increasing frequency, which can be fitted to a critical power law for SSG [16],

$$\tau = 1/(2\pi f) = \tau^*(T_p/T_g - 1)^{-z\nu} \tag{1}$$

where τ^* is the relaxation time of individual particle moment, T_g is the static glass temperature and $z\nu$ is the dynamic critical exponent. Our data can be fitted well by Eq. (1) with $\tau^* \approx 10^8$ s, $z\nu \approx 9.7$ and $T_g \approx 52$ K [inset of Fig. 1(b)]. These values are close to those reported for SSG ($\tau^* \approx 10^8$ s and $z\nu \approx 10.2$) [17]. Furthermore, the memory effect of SSG state has also been observed in NiMnIn13 [14].

The CEB effect after FC is observed in all NiMnInx ($x = 11$, 12, 13, 14 and 15) bulk alloys [14]. Here, we investigate the $M(H)$ loops at 10 K after ZFC from an unmagnetized state in these alloys. The unmagnetized initial state at 10 K in these alloys can be obtained easily if they are zero-field cooled from 300 K due to their T_cs are lower than 300 K [14]. Figure 1(c) shows the P type $M(H)$ of NiMnIn13 at 10 K after ZFC from 300 K with maximum measurement field $|H_m^{max}| \, (= |+H| = |-H|) = 40$ kOe. The dashed line shows the initial magnetization curve, which lies outside the major hysteresis loop. The magnetization at the starting point of the initial magnetization curve ($H = 0$) is zero, indicating that the initial state at 10 K is an unmagnetized state [14]. It is worth noting that the ZFC $M(H)$ loop shows a *large* shift along the magnetic field axis, which has never been observed in any previous CEB systems. The equal magnetization values in the highest positive and
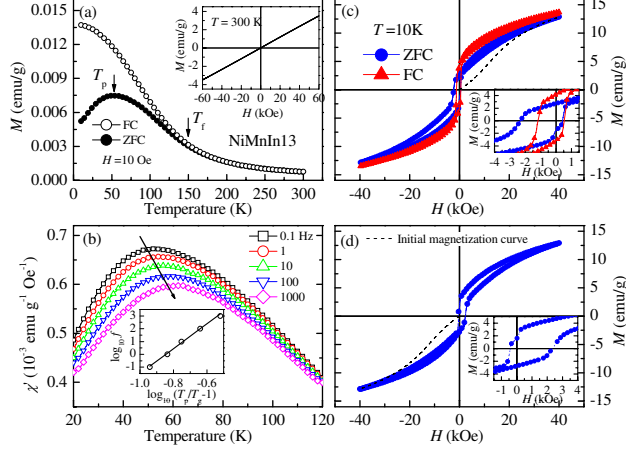
FIG. 1. (color online) (a) $M(\mathrm{T})$ curves measured under $H = 10$ Oe after ZFC and FC. The inset shows the $M(\mathrm{H})$ curve at 300 K. (b) Temperature dependence of the real part of the ac susceptibility measured at frequencies $f = 0.1, 1, 10, 100, 1000$ Hz with ac magnetic field of 2.5 Oe after ZFC from 300 K. The inset shows the plot of $\log_{10} f$ vs $\log_{10}(T_{\mathrm{p}}/T_{\mathrm{g}} - 1)$ (open circles) and the best fit to Eq. (1) (solid line). (c) and (d) $M(\mathrm{H})$ loops of NiMnIn13 at 10 K with $|H_{\mathrm{m}}^{\max}| = 40$ kOe after ZFC and FC ($H = 40$ kOe) from 300 K. The dashed lines show the initial magnetization curves. The insets show the larger scale at the low field.

negative magnetic fields indicate the shifted loop is not a nonsymmetrical minor hysteresis loop [14]. We also measured the N type $M(\mathrm{H})$ loops with opposite direction of the initial magnetization field at 10 K after ZFC [Fig. 1(d)] [14], which shift to the positive magnetic field axis showing a centrally symmetric image of the P type $M(\mathrm{H})$ loops. This result cannot be expected from the effect of remanent field of superconductor magnet/remanent magnetization of the samples, in which the shift direction of $M(\mathrm{H})$ loop is independent of the direction of the initial magnetization field. Furthermore, both the EB field (H_{EB}) and coercivity (H_{c}) after ZFC can be larger than those after FC [Fig. 1(c)] [14], which indicates that the EB after ZFC in the present case is not a spontaneous EB [10]. The H_{EB} and H_{c} are defined as $H_{\mathrm{EB}} = -(H_{\mathrm{L}} + H_{\mathrm{R}})/2$ and $H_{\mathrm{c}} = -(H_{\mathrm{L}} - H_{\mathrm{R}})/2$, respectively, where H_{L} and H_{R} are the left and right coercive fields. To further confirm this phenomenon after ZFC, we measured the temperature dependence of H_{EB} and H_{c} for $|H_{\mathrm{m}}^{\max}| = 40$ kOe and the training effect at 10 K for several selected $|H_{\mathrm{m}}^{\max}|$s [14], which are similar to those in the CEB systems obtained after FC [5, 18]. The key difference is that EB in NiMnIn13 can be observed after *ZFC from an unmagnetized state*. Namely, FM unidirectional anisotropy,
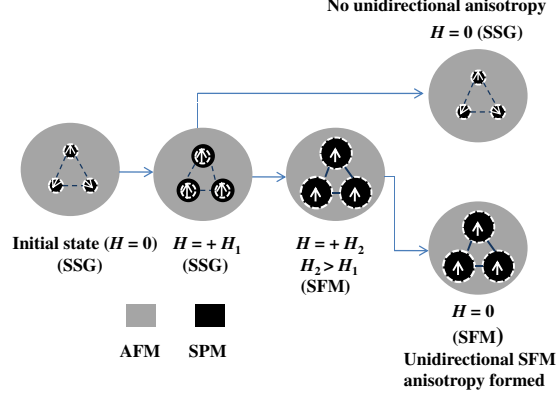
4

FIG. 2. (color online) Simplified schematic diagrams of the evolution of the SPM domains embedded in an AFM single domain (AFM anisotropy axis is parallel to the direction of applied magnetic field) under external magnetic field at temperature below T_B. The initial magnetic state after ZFC is a SSG state. The white arrows represent that the superspin direction of SPM domains. The dashed white circles show the coupling interfaces of SPM-AFM. The dashed blue lines represent that the coupling of SPM domains is a glassy coupling, while the solid blue lines represent the coupling of SPM domains is a SFM exchange.

usually obtained by FC from higher temperature, can be induced *isothermally* during the initial magnetization process.

To investigate its origin, we consider the evolution of the initial magnetic state of NiMnIn13 after ZFC under external magnetic field as shown in Fig. 2. It is a simplified schematic diagram with SPM domains embedded in an AFM single domain (AFM anisotropy axis is parallel to the direction of applied magnetic field). The applied magnetic field aligns all the SPM domains along the direction of external field. When the Zeeman energy of AFM spins (J_{ZE}, which is proportional to the magnitude of magnetic field) near the interface is larger than the coupling energy of SPM-AFM at the interface (J_{int}, constant) and their anisotropy energy (constant), the applied field will align these AFM spins along the direction of external field [19]. Therefore, the SPM domains will grow in size. However, the enlarged SPM domains are at metastable state and the coupling interface of SPM-AFM remains unchanged at this stage [see the dashed white circles in Fig. 2]. After removal of external magnetic field, they will shrink and return to their initial sizes due to the AFM anisotropy energy.

The growth of SPM domain size will decrease the inter-domain distance, thus increases

the interaction between SPM domains. This is similar to the process of increasing the concentration of SPM nanoparticles in the conventional SSG systems [16]. When the interaction between SPM domains reaches the critical value, the coupling of SPM domains will become superferromagnetic (SFM) exchange through tunnelling superexchange [16]. The difference between SFM and conventional FM is that the atomic spins in the conventional FM are replaced by the superspins of SPM domains. *The formation of SFM exchange may change the internal interaction of each enlarged SPM domain (metastable at SSG state) such that they become stable as shown in Fig. 2.* [While in the case of SPM *nanoparticles* embedded in AFM matrix with a chemical interface (different materials) [6], the SPM nanoparticles cannot grow to form larger stable particles at the expense of AFM matrix]. As a result, a *new stable* SFM-AFM interface with unidirectional moment of SFM is formed and will pin the SFM superspins below the blocking temperature (T_B), which is similar to an FM-AFM interface with unidirectional FM spins formed after FC in the CEB systems. The difference is that in the present case the SFM-AFM interface is induced isothermally by external magnetic field. While in the CEB systems it is usually reconfigured under FC. According to this model, the moment of SPM domains increases with increasing size under external magnetic field. We have only considered AFM domains with anisotropy axis parallel to external magnetic field in this model. For AFM domains with anisotropy axis non-parallel to external magnetic field, there is an angle between the direction of the initial magnetization field and the anisotropy axis. This configuration can still result in EB effect, which is similar to the EB effect in the CEB systems with different angles between the direction of the cooling field and the AFM anisotropy axis [20]. Based on the above analyses, we believe that a SFM unidirectional anisotropy, which is similar to an FM unidirectional anisotropy, can be formed during the initial magnetization process.

In order to confirm this model, we further measured the $M(H)$ loops with various magnitudes of the initial magnetization fields (different $|H_m^{max}|$s) at 10 K after ZFC from 300 K [14]. Figure 3(a) shows H_{EB} and H_c as a function of $|H_m^{max}|$. There is a critical $|H_m^{max}|$ (H^{crit}) = 30 kOe, at which H_{EB} reaches the maximum value and H_R remains almost constant at higher $|H_m^{max}|$ [Fig. 3]. The maximum H_{EB} means the formation of the maximum FM unidirectional anisotropy [5]. Thus, the meaning of H^{crit} is that at which SSG state completely transforms to SFM state, producing maximum SFM unidirectional anisotropy. The decrease of the H_{EB} at higher $|H_m^{max}|$ is only due to the decrease of the H_L [Fig. 3(b)], which may
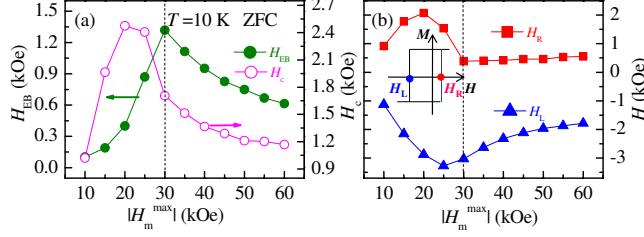
6

FIG. 3. (color online) (a) H_{EB} (left) and H_c (right) as a function of $|H_m^{max}|$ in NiMnIn13 at 10 K after ZFC. (b) The left (H_L) and right (H_R) coercive fields as a function of $|H_m^{max}|$. Inset shows the definition of H_L and H_R in a $M(H)$ loop. The dotted lines show the position of $H^{crit} = 30$ kOe.

originate from the change of bulk AFM spin structure under large applied magnetic field [14]. The bulk AFM spin structure has been shown to play a crucial role in EB effect in thin film system [21].

When $|H_m^{max}| < H^{crit}$, only part of the SSG state transforms to the SFM state during the initial magnetization process. For SSG state, there is a remnant magnetization and H_c in $M(H)$ loops due to irreversible switching of a collective state [17]. The H_c (both H_L and H_R) increases with increasing $|H_m^{max}|$ (a series of minor hysteresis loops). However, the number of SPM domains at SSG state will decrease with increasing $|H_m^{max}|$ due to more SSG state transforming to SFM state, which generates more new interfaces with SFM unidirectional anisotropy. Thus, the H_{EB} increases with increasing $|H_m^{max}|$ at this stage, leading to the increase of coercive field in one direction (H_L) and the decrease in the other (H_R). The final coercive fields are attributed to a combined effect of SPM domains in SSG and SFM states. Due to the opposite $|H_m^{max}|$ dependence for these two effects, the H_R reaches maximum at a field smaller than H^{crit}. For H_L, both effects have the same $|H_m^{max}|$ dependences, resulting in a continuous increase of H_L with $|H_m^{max}|$. As a result, the field, at which H_c reaches maximum, is smaller than the H^{crit} of H_{EB}. Further supports to the model shown in Fig. 2 are provided in the supplementary information including anomalous remanent magnetization dependence of EB effect, isothermal tuning of EB after ZFC from an unmagnetized state, and strong cooling field dependence of CEB effect in NiMnIn13 [14].

Finally, we have further verified the model by changing the size of the initial domains, which is crucial to the formation of the SFM unidirectional anisotropy [14]. If the size of the initial domains is larger than the critical value, SFM or FM domains will form and no EB effect will appear after ZFC [13]. Figure 4(a) shows the $M(H)$ curves of NiMnInx at 10 K.
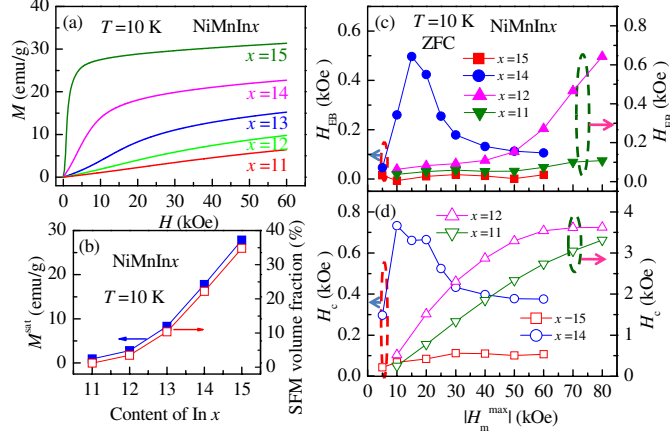
FIG. 4. (color online) (a) Field dependence of magnetization of NiMnInx at 10 K. (b) Saturation magnetization (M^{sat}) and SFM volume fraction as a function of In content at 10 K. (c) and (d) $|H_{\text{m}}^{\text{max}}|$ dependence of H_{EB} and H_{c} at 10 K for $x = 11$, 12 (right), and 14, 15 (left).

The saturation magnetization of NiMnInx increases with increasing In content [Fig. 4(b)], which is consistent with the previous results [22]. The T_{c}s of these alloys are lower than 300 K and the T_{N} decreases continuously with increasing In content [14]. The saturation magnetization of NiMnInx at 10 K is very small compared with that of the stoichiometric compound Ni$_{50}$Mn$_{25}$In$_{25}$ (80 emu/g, pure FM state at low temperatures) [22]. The decrease of saturation magnetization in the off-stoichiometric alloys is due to the excess of Mn atoms occupying a number of In sites, which produces AFM coupling [22]. The SFM (may include some SPM or FM domains) volume fraction increases from $\sim$1 % in NiMnIn11 to $\sim$35 % in NiMnIn15 at 10 K [Fig. 4(b)]. Thus, the average domain size in $x = 14$ alloy is larger than that of NiMnIn13 at the initial state. The larger size of SPM domain makes the $H^{\text{crit}} = 15$ kOe, at which all of the SSG state transforms to SFM state, being smaller than that of NiMnIn13 [Fig. 4(c)]. Furthermore, the SFM volume fraction in $x = 14$ alloy is about 22 % (the total volume fraction of SPM/SFM in the initial state is less than this value), which is close to the threshold concentration for percolation in three dimensional system ($\sim$16 %) [23]. The SFM domains no longer separate from each other in AFM matrix at larger volume fraction resulting in the formation of FM domains at $x > 14$. For $x = 15$ alloy, there is no SPM domains at the initial state and the M(H) loops after ZFC shows double-shifted behavior with no EB effect, which is similar to the results of NiMnIn16 [13, 14]. For $x = 11$ and 12, the continuous increase of H_{EB} with $|H_{\text{m}}^{\text{max}}|$ up to 80 kOe is due to the smaller size

of SPM domain, which is similar to results of NiMnIn13 for $|H_{\mathrm{m}}^{\mathrm{max}}| < H^{\mathrm{crit}}$. Large H_{c} has also been observed for $x = 11$ and 12 and the H_{c} of NiMnIn12 shows tendency to maximum value at higher $|H_{\mathrm{m}}^{\mathrm{max}}|$s prior to the maximum of H_{EB} [Fig. 4(d)]. All of these results are consistent to the discussions in NiMnIn13 within the model as shown in Fig. 2.

In summary, we have observed a large EB effect after ZFC from an unmagnetized state in Ni-Mn-In bulk alloys, exhibiting the same relationship of the temperature dependence of H_{EB} and H_{c}, and the training effect as in the CEB systems after FC. Such phenomenon is attributed to a SFM unidirectional anisotropy formed during the initial magnetization process. These results will open a new direction to realize EB effect.

* MLiuY@ntu.edu.sg

† WangLan@ntu.edu.sg

[1] W. H. Meiklejohn and C. P. Bean, Phys. Rev. **102**, 1413 (1956).

[2] M. Ali *et al.*, Nat. Mater. **6**, 70 (2007).

[3] G. Salazar-Alvarez *et al.*, J. Am. Chem. Soc. **129**, 9102 (2007).

[4] W. C. Cain and M. H. Kryder, J. Appl. Phys. **67**, 5722 (1990).

[5] J. Nogués and I. K. Schuller, J. Magn. and Magn. Mater. **192**, 203 (1999).

[6] J. Nogués *et al.*, Phys. Rep. **422**, 65 (2005).

[7] D. Engel *et al.*, J. Magn. and Magn. Mater. **293**, 849 (2005).

[8] N. J. Gokemeijer and C. L. Chien, J. Appl. Phys. **85**, 5516 (1999).

[9] P. Miltényi *et al.*, Appl. Phys. Lett. **75**, 2304 (1999).

[10] J. Saha and R. H. Victora, Phys. Rev. B **76**, 100405 (2007).

[11] Z. Li *et al.*, Appl. Phys. Lett. **91**, 112505 (2007).

[12] M. Khan *et al.*, Appl. Phys. Lett. **91**, 072510 (2007).

[13] B. M. Wang *et al.*, J. Appl. Phys. **104**, 043916 (2008).

[14] See supplementary information.

[15] D. Y. Cong *et al.*, Appl. Phys. Lett. **96**, 112504 (2010).

[16] S. Bedanta and W. Kleemann, J. Phys. D: Appl. Phys. **42**, 013001 (2009).

[17] S. Sahoo *et al.*, Appl. Phys. Lett. **82**, 4116 (2003).

[18] M. K. Chan *et al.*, Phys. Rev. B **77**, 014420 (2008).

[19] C. Leighton *et al.*, Phys. Rev. B **60**, 12837 (1999).

[20] J. Nogués *et al.*, Phys. Rev. B **59**, 6984 (1999).

[21] R. Morales *et al.*, Phys. Rev. Lett. **102**, 097201 (2009).

[22] T. Krenke *et al.*, Phys. Rev. B **73**, 174413 (2006).

[23] H. Scher and R. Zallen, J. Chem. Phys. **53**, 3759 (1970).